Cross sections for electron collisions with NF_3

Biplab Goswami, Rahla Naghma, and Bobby Antony
Department of Applied Physics, Indian School of Mines, Dhanbad 826004, Jharkhand, India
(Received 31 July 2013; published 25 September 2013)

A comprehensive calculation of electron impact scattering by NF_3 molecule is reported in this article. Total cross sections were presented over electron impact energies from 1 eV to 5 keV. The *ab initio* *R*-matrix method was employed through QUANTEMOL-N software for low-energy calculations and spherical complex optical potential formalism for intermediate to high-energy calculations. The consistency of data at the overlapping energy (∼14 eV) from these theories allows us to predict total cross sections for such an extensive energy range. Electronic excitation, rotational excitation, and differential cross sections were calculated using the *R*-matrix method at low incident energies. In the present study, resonances were detected at 5.6 and 6.2 eV, indicating the probability of anions formation by the electron attachment process and further decay to neutral and negative ion fragments. In general, the present results show overall agreement with previous theories and experiments, wherever available. A maiden attempt to calculate e-NF_3 rotational excitation cross sections is also undertaken.

DOI: 10.1103/PhysRevA.88.032707 PACS number(s): 34.80.Bm, 34.80.Gs, 34.80.Ht

I. INTRODUCTION

Trifluoramine (NF_3) is an electron-attaching gas, primarily employed in industry for the cleaning of chemical vapor deposition chambers in the high-volume production of liquid crystal displays, silicon-based thin film solar cells, and plasma etching of silicon wafer [1]. It is an efficient fluorine source in the manufacturing of very large scale integrated circuits [2] and in rare gas halide excimer laser systems [3]. The growing number of applications for this molecule in the advancement of new technology leads to further concern about the anthropogenic effect of this molecule in the atmosphere. Recently NF_3 was included in the greenhouse gases recognized by the group of Kyoto with an atmospheric lifetime of 740 years [4]. It can trap 17 000 times more heat per molecule than that of CO_2 in the atmosphere when compared over a period of 100 years [4,5]. So a detailed knowledge of gas phase properties, particularly electron interaction dynamics, of NF_3 over a wide range of energy is required.

Nevertheless, only a few attempts have been made to investigate the electron interactions with NF_3 molecule. The measurements of total cross section (TCS) for electron impact by NF_3 molecule were performed by Szmytkowski *et al.* [6] using the linear transmission technique at energies between 0.5 and 370 eV. Shi *et al.* [7] reported the theoretical TCS data over the energy range 30 and 5000 eV using the modified additivity rule method. TCS are also computed by Rahman *et al.* [8] using the spherical complex optical potential formalism in the energy range 15–2000 eV.

Previous studies on elastic and differential cross sections include those of Rescigno [9], Boesten *et al.* [10], and Joucoski and Bettega [11]. Rescigno [9] reported the results of *ab initio* calculation utilizing complex Kohn variational technique in the 0–25 eV energy range, Boesten *et al.* [10] measured the cross sections using the cross-beam technique in the energy range 1.5–100 eV, while Joucoski and Bettega [11] performed calculations applying the Schwinger multichannel (SMC) method for the energies between 2 and 60 eV. The ionization cross sections for NF_3 by electron scattering in the energy range 14–200 eV were measured by Haaland *et al.* [12] and Tarnovsky *et al.* [13] using Fourier transform mass spectrometry and the fast beam technique, respectively. Deutsch *et al.* [14] computed the ionization cross section from the ionization threshold to 200 eV by employing DM formalism. Finally, Rahman *et al.* [8] reported both theoretical and measured ionization cross sections by employing spherical complex optical potential formalism and time of flight mass spectrometry techniques respectively over energy ranging between 15 and 500 eV. A summary of the literature survey for e-NF_3 scattering is given in Table I.

As suggested earlier, the electron scattering studies with NF_3 are fragmentary and are restricted to a small energy range. Cross section data for different scattering channels covering a wider energy domain are still lacking. In this study electron impact TCSs for NF_3 were reported over an extensive range of incident electron energies from 1 to 5000 eV by combining two theoretical methods in different energy regions. For low incident energies typically below 15 eV, calculations were carried out using the *R*-matrix method through QUANTEMOL-N (QMOL) software [15], while above the ionization threshold of the target molecule the spherical complex optical potential (SCOP) [16–18] formalism is employed. The results obtained by the two formalisms were found to merge at the overlapping energy, enabling us to predict cross section data over a broad energy range. In addition to this, the present study focuses on identifying the low-lying shape resonance and fragmentation path via dissociative electron attachment at low impact energies. Resonances are sudden amplification in the TCS due to formation of transient anion by the temporary trapping of the impinging electron inside the molecule at specific energy that leads to the decay of anion into neutral and anionic fragments.

The organization of the paper is as follows. Section II describes the theoretical methodologies employed in the calculations. Section III presents the results and discussions of the present study. Finally, Section IV summarizes and concludes this work.

II. THEORETICAL METHODOLOGY

The present article reports the total cross section by employing two distinct methodologies, *viz.*, the *R*-matrix

TABLE I. Review of literature for e^--NF_3 scattering.

Energy Range (eV)	Cross section	Reference	Method (Expt.: experimental; Theor.: theoretical)
0–25	DCS, excitation	Rescigno [9]	Complex Kohn variational calculations
4–60	Elastic, DCS	Joucoski and Bettega [11]	SMC method (Theor.)
0.5–370	TCS, ionization	Szmytkowski *et al*. [6]	Linear transmission technique (Expt.)
1.5–100	Elastic, DCS	Boesten *et al*. [10]	Crossed-beam technique (Expt.)
15–2000	TCS,	Rahman *et al*. [8]	Spherical complex optical potential (Theor.)
	Ionization		Spherical complex optical potential (Theor.) Time of flight mass spectrometry (Expt.)
30–5000	TCS	Shi *et al*. [7]	Modified additivity rule (Theor.)
14–200	Ionization	Haaland *et al*. [12]	Fourier transform mass spectrometry (Expt.)
14–200	Ionization	Tarnovsky *et al*. [13]	Fast beam technique (Expt.)
14–200	Ionization	Deutsch *et al*. [14]	DM formalism (Theor.)

method and the SCOP formalism, which are applicable in two distinct regimes of impact energy. The former is suited for low incident energies below the ionization threshold of the target and the latter above the threshold. Before going into the details of the theoretical formalism, a discussion of the target model adopted for low-energy calculations is also presented.

A. Target model

NF_3 is a trigonal pyramidal molecule. All calculations in this work are carried out at the equilibrium geometry of the target with N-F bond length 1.365 Å and F-N-F angle 102.37° [19] in the reduced symmetry C_S (instead of C_{3v} point group). The double zeta plus polarization (DZP) basis set is used to construct the target wave functions. The ground state Hartree-Fock electronic configuration is represented as $1a'^2$, $1a''^2$, $2a'^2$, $3a'^2$, $4a'^2$, $5a'^2$, $2a''^2$, $6a'^2$, $7a'^2$, $3a''^2$, $8a'^2$, $9a'^2$, $4a''^2$, $10a'^2$, $5a''^2$, $6a''^2$, $11a'^2$. Out of these 34 target electrons, 14 electrons are frozen in $1a'$, $2a'$, $3a'$, $4a'$, $5a'$, $1a''$, $2a''$ molecular orbitals, and the remaining 20 electrons are kept in the active space of $6a'$, $7a'$, $8a'$, $9a'$, $10a'$, $11a'$, $12a'$, $3a''$, $4a''$, $5a''$, $6a''$, $7a''$ molecular orbitals. A total number of 583 configuration state functions (CSFs) are generated for the representation of four target states for the ground state, and the number of channels included in the calculation is 50.

By employing the present target model, calculation yields a ground state energy of −352.669 hartree, which is in excellent agreement with the previous theoretical values of −352.65526 hartree of Rescigno [9] and −352.678856 hartree reported in the Computational Chemistry Comparison and Benchmark Database (CCCBDB) [19]. The rotational constant obtained in the calculation is 0.359 cm^{-1}, which agrees well with the experimental value of 0.35628 cm^{-1} reported by Novick *et al*. [20]. The present computed dipole moment 0.1156 a.u. matches well with the theoretical value of 0.111 a.u. [9] and is in reasonable agreement with the experimental value of 0.093 a.u. [21]. The first electronic excitation energy of 8.5 eV obtained in the present calculation matches very well with the computed value of 8.32 eV reported by Rescigno [9]. The target properties along with the available comparison are summarized in Table II.

B. Low-energy formalism (1 to ∼15 eV)

Considerable progress have been made over the past few decades in developing accurate theoretical methods for computing low-energy electron molecule cross sections, and perhaps the *ab initio* *R*-matrix method is the most widely used approach. The underlying principle behind the *R*-matrix method is the division of configuration space into two spatial regions, an inner region and an outer region. Here the inner region is a sphere of radius 10 a.u. centered at the center of mass of the target molecule. This choice of the inner region (*R*-matrix) radius is made such that the inner sphere envelops the total wave functions of all the target states included in the calculations. Inside the inner region, the scattering electron and target electrons are indistinguishable, this making the problem numerically complex but very accurate. The interaction potential dominating in this region comprises static, exchange, and correlation polarization potentials, which are short range in nature. The inner region problem is solved by employing rigorous quantum chemistry code and takes maximum computational time and resource in the calculation. Moreover, the inner region problem is solved only once as it does not depend on the energy of the scattering electron. However, in the outer region, where the scattering electron is at

TABLE II. Target properties.

Properties of NF_3	Present	Experimental	Theoretical
Ground-state energy (hartree)	−352.669	–	−352.678856 [19] −352.65526 [9]
First excitation energy (eV)	8.5330	–	8.32 [9]
Rotational constant (cm^{-1})	0.3590	0.35628 [20]	–
Dipole moment (a.u.)	0.1156	0.093 [21]	0.111 [9]

a large distance from the center of mass of the target, only long-range multipolar interactions between the scattering electron and various target states are included. Here the problem is solved by a single center close coupling approximation, which gives a quick and fast solution. Presently all the calculations were performed within the fixed nuclei approximation at the equilibrium geometry of the target.

The inner region wave function is constructed using the close-coupling (CC) approximation [22], which is used to solve the time-independent Schrödinger equation. The inner region wave function can be expressed as

$$\psi_k^{N+1} = A \sum_I \psi_I^N(x_1, \ldots, x_N) \sum_j \xi_j(x_{N+1}) a_{Ijk} + \sum_m \chi_m(x_1, \ldots, x_{N+1}) b_{mk}, \quad (1)$$

where A is the antisymmetrization operator which ensures the indistinguishability between the scattering and target electrons, ξ_j is a continuum orbital spin coupled with the scattering electron, x_N is the spatial and spin coordinate of the Nth electron, and a_{Ijk} and b_{mk} are variational coefficients. The target plus continuum states are used in the close-coupled expansion, and the static exchange calculation has a single Hartree-Fock target state in case of first summation. The second summation runs over configurations χ_m, where all electrons are placed in target molecular orbitals. The close-coupled calculation uses the lowest number of target states, represented by a configuration interaction (CI) expansion in the first term and more than 100 configurations in the second including the orthogonality relaxation and short-range polarization effects.

The complete molecular orbital representation in terms of occupied and virtual molecular target orbitals is constructed using the Hartree-Fock self-consistent field method with Gaussian-type orbitals and the continuum orbitals of Faure *et al.* [23] and included up to g orbital ($l = 4$). The effect of partial wave for $l > 4$ is included using the Born correction approach at all energies. The R matrix acts as a link between the inner region and outer region. The R matrix computed at the boundary of the inner region is propagated to large scattering distance, where the radial equation describing the scattering electron can be matched with the analytical expressions given by Gailitis [24]. This matching gives K matrices, which are diagonalized to obtain the eigenphase sum. The eigenphase sum is further used to obtain the position and width of the resonances. The K matrices are also used to determine T matrices by the definition

$$T = \frac{2iK}{1 - iK}. \quad (2)$$

These T matrices are in turn used to calculate various cross sections. The DCS are determined using the POLYDCS program of Sanna and Gianturco [25].

C. High-energy formalism

To study the interaction of intermediate to high-energy electrons with NF_3 molecule, the well-established SCOP formalism is employed. Within the fixed nuclei approximation, the electron molecule interaction dynamics is represented by a complex optical potential consisting of real (V_R) and imaginary (V_I) parts,

$$V_{\text{opt}}(r, E_i) = V_R(r) + iV_I(r, E_i) = V_{\text{st}}(r) + V_{\text{ex}}(r, E_i) + V_p(r, E_i) + iV_{\text{abs}}(r, E_i). \quad (3)$$

Here the real part of the interaction potential comprises of static (V_{st}), exchange (V_{ex}), and polarization (V_{pol}) contributions. The model potentials representing these terms are formulated by using molecular charge density and target parameters, *viz.*, ionization potential and static electric dipole polarizability as input. The molecular charge density is in turn determined from the atomic charge densities of the constituent atoms derived from the parameterized Hartree-Fock wave functions of Cox and Bonham [26]. The static potential arises due to coulomb interaction between the target and incoming electron and is also formulated using parameterized Hartree-Fock wave functions given by Cox and Bonham [26]. The exchange potential accounts for the indistinguishability between the incoming and target electrons and is derived from the parameter-free Hara's free electron gas exchange model [27]. The polarization potential represents dynamical response of target molecule to the impinging electron, i.e., the short range correlation and long range polarization effect and is described by the parameter-free model of correlation-polarization potential given by Zhang *et al.* [28]. Here an asymptotic form of polarization potential is used by incorporating various multipole nonadiabatic corrections into the intermediate region. Finally, the imaginary part in V_{opt} is represented by the absorption potential V_{abs}, which accounts for the electron induced inelastic scattering processes except rotation and vibration. Here these nonspherical terms were neglected, as they are not significant at the present energy range. The absorption potential is given

by the quasi-free model potential of Staszewska *et al.* [29] as

$$V_{\text{abs}}(r,E_i) = -\rho(r)\sqrt{\frac{T_{\text{loc}}}{2}}\left(\frac{8\pi}{10k_F^3E_i}\right)\theta\left(p^2-k_F^2-2\Delta\right) \times (A_1+A_2+A_3), \tag{4}$$

where the parameters A_1, A_2, and A_3 are defined as

$$A_1 = \frac{5k_f^3}{2\Delta};\ A_2 = -\frac{k_f^3\left(5p^2-3k_f^3\right)}{\left(p^2-k_f^2\right)^2}$$

and

$$A_3 = 2\theta\left(2k_f^2+2\Delta-p^2\right)\frac{\left(2k_f^2+2\Delta-p^2\right)^{5/2}}{(p^2-k_f^2)^2}.$$

The local kinetic energy of the incident electron can be expressed as

$$T_{\text{loc}} = E_i - (V_{\text{st}}+V_{\text{ex}}+V_{\text{pol}}). \tag{5}$$

Here the momentum and Fermi wave vector of the electron are represented by $p=[2E_i]^{1/2}$ and $k_f=[3\pi^2\rho(r)]^{1/3}$, respectively. The functions A_1, A_2, and A_3 depend on the Heaviside unit step function, $\theta(x)$ ionization threshold (I), energy parameter Δ, and E_i as shown in Eq. (4). The parameter Δ is the principle factor that limits the effect of inelastic processes and is defined as the threshold below which inelastic processes are not permissible. In the original Staszewska model [29] $\Delta = I$ is considered; however, Δ fixed at I would not allow excitation at energies $E_i \leqslant I$. Due to this fact, here Δ is assumed to be a gradually varying function of energy near the ionization potential of the target, with first excitation as the lower limit [16].

The radial Schrödinger equation for e^- -NF_3 interaction is solved by incorporating the full complex optical potential, given in Eq. (3), using the method of partial wave analysis. The solutions of the scattering equation are obtained in the form of complex phase shifts (δ_l) for each partial wave. This phase shift contains the signature of interaction of the incoming electron with the target molecule. Only few partial waves are significant at low energies, but as the impact energy increases, more partial waves are required for convergence. The complex phase shift thus obtained is employed to calculate the inelasticity or absorption factor through

$$\eta_l = \exp(-2\text{Im}\delta_l), \tag{6}$$

which is further used to find the relevant cross sections, *viz.*, Q_{el} and Q_{inel} cross sections [30] employing the expressions given below:

$$Q_{\text{inel}}(E_i) = \frac{\pi}{k^2}\sum_{l=0}^{\infty}(2l+1)\left(1-\eta_l^2\right) \tag{7}$$

and

$$Q_{el}(E_i) = \frac{\pi}{k^2}\sum_{l=0}^{\infty}(2l+1)\left|\eta_l\exp(2i\text{Re}\,\delta_l)-1\right|^2. \tag{8}$$

The total cross section is the sum of these two cross sections.

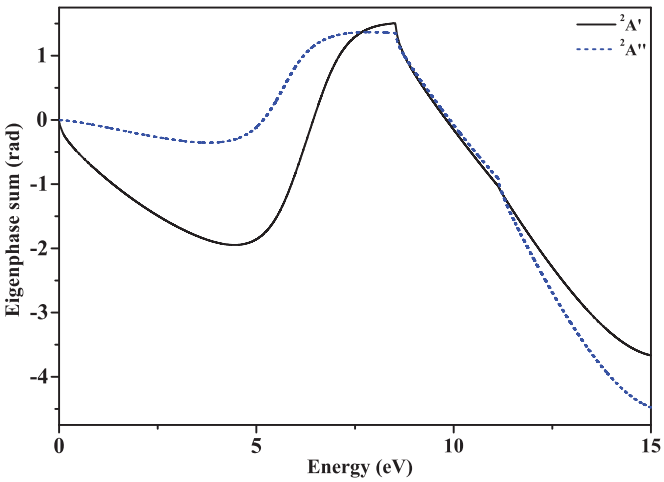

FIG. 1. (Color online) Doublet eigenphase sum for NF_3.

III. RESULTS AND DISCUSSION

The electron impact total cross section for the NF_3 molecule over the energy range from 1 to 5000 eV is presented here. The results obtained by employing two distinct formalisms will be tested for consistency at the overlapping energy. In addition to the TCS, electronic excitation, rotational excitation, and differential cross sections calculated by the close coupling R-matrix method are also presented. The present study has identified resonance features at low energies. The results are presented in graphical form in Figs. 1–6 and compared with the existing data. The total cross section data are tabulated in Table III.

The eigenphase sum diagram for the reduced C_s symmetry (doublet scattering states $^2A'$ and $^2A''$) of NF_3 is shown in Fig. 1. At low energies, the study of the eigenphase sum is significant as it helps to localize the position of resonances. The position of the resonances is located by identifying the energy at which the eigenphase sum goes through zero. Resonance is predominantly indicative of the dissociative electron attachment phenomenon, where the short lived anion formed by temporarily trapping the projectile electron to the molecule decays into neutral and charged fragments before the electron auto detaches. Another possible scattering channel

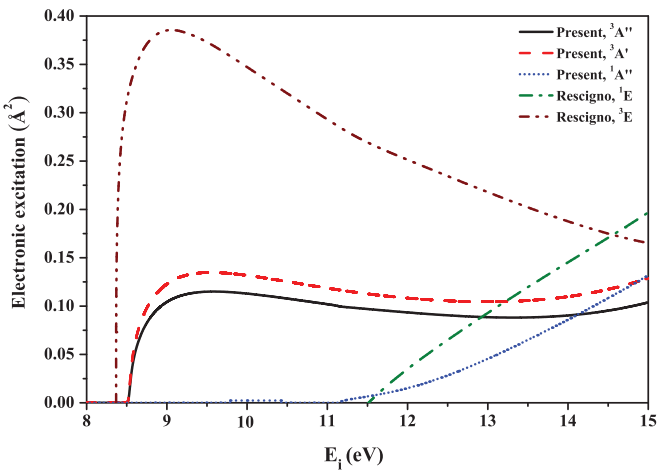

FIG. 2. (Color online) Electronic excitation cross section for e-NF_3 scattering.

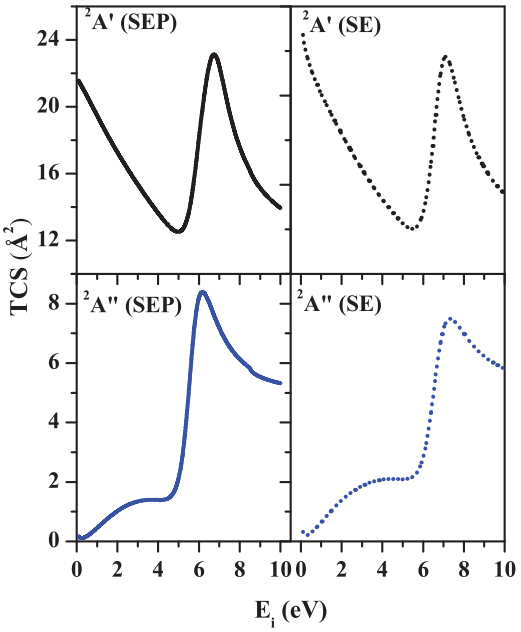

FIG. 3. (Color online) Symmetry component of the elastic cross section for electron scattering by NF_3.

is corresponding to the ejection of attached electron back to the continuum leaving the molecule in the vibrational excited state. However, Ruckhaberle *et al.* [31] have reported that electron attachment in the energy range 0–10 eV by gas phase NF_3 is purely dissociative and yields the ionic fragments F^-, F_2^-, and NF_2^-. Although resonances can be a combination of shape, Feshbach, and core excited in character, it is not really possible to predict how much each one makes up a resonance. However, in the present study we observe a broad resonance, which is the characteristic of shape resonance. The electron scattering with NF_3 molecule at energies well below the ionization threshold presented in Fig. 1 shows clear signature of resonances. Also, it is clear from the figure that the curves for both symmetries change sign at different energies. This indicates the contribution of different symmetries to the total cross section. The eigenphase sum for both symmetries shows a discontinuity at about 9 and 11 eV exhibiting nondegeneracy, which corresponds to the opening of more scattering channels. It is worth noting here that the ionization potential of NF_3 is around 13 eV. $^2A''$ symmetry shows a rapid increment towards the positive eigenphase sum crossing at about 5.6 eV, which is in excellent agreement with the shape resonance located in the elastic momentum transfer cross section at 5.5 eV reported by Rescigno [9]. Similarly $^2A'$ symmetry gives a resonance at 6.2 eV, which is close to the earlier reported value of 7 eV by Joucoski and Bettega [11]. They found two closely spaced shape resonances around 7 eV belonging to A and E representation of the C_{3v} group. This shift in the position of resonance may have occurred due to the absence of polarization effect in their calculations. The presence of resonances is contemplated as sharp peak in the TCS curve as well.

Figure 2 displays electronic excitation cross sections from ground state to excited states $^3A''$, $^3A'$, and $^1A''$ along with ^1E and ^3E excited state of Rescigno [9]. It can be seen from the graph that the threshold of the first electronic excitation ($^3A''$ and $^3A'$ states) is at 8.53 eV and that of the $^1A''$ state is around 11 eV. The vertical excitation energies obtained by Rescigno [9] for ^3E and ^1E states (C_{3v} point group symmetry) in CI calculations were 8.32 and 11.41 eV, respectively. Even though the present calculations were carried out in the reduced C_s symmetry instead of C_{3v}, the values obtained for electronic excitation energies are in reasonable agreement with the theoretical values of Rescigno [9].

Elastic cross sections for the symmetry component for static exchange (SE) and static exchange plus polarization (SEP) model in the energy range 0–10 eV are presented in Fig. 3. It is clear from the figure that the inclusion of polarization potential slightly pushes the location of resonance towards the lower energies.

Figure 4 illustrates the variation of present total cross section for e-NF_3 scattering with electron energy. The present TCS is compared with the measurement of Szmytkowski *et al.* [6] and theoretical data of Shi *et al.* [7]. Since only two data sets are available for comparison, two more computed values [6] are also plotted in Fig. 4. The first one is the computed TCS (Theor.), which is the sum of the theoretical integral elastic cross section of Joucoski and Bettega [11] up to 60 eV and Szmytkowski *et al.* [6] above it and ionization cross section of Szmytkowski *et al.* [6]. The second one is called the computed TCS (Expt.), which is the sum of the experimental electron attachment cross section of Nandi *et al.* [32], elastic cross section of Boesten *et al.* [10] and ionization cross section of Haaland *et al.* [12]. In the low-energy region, TCSs for both SE and SEP models are presented. The present low energy TCS is expressed as the sum of elastic, electronic excitation, and rotational excitation cross sections. The present TCS curve shows prominent enhancement at 6.6 eV, which is in good comparison with

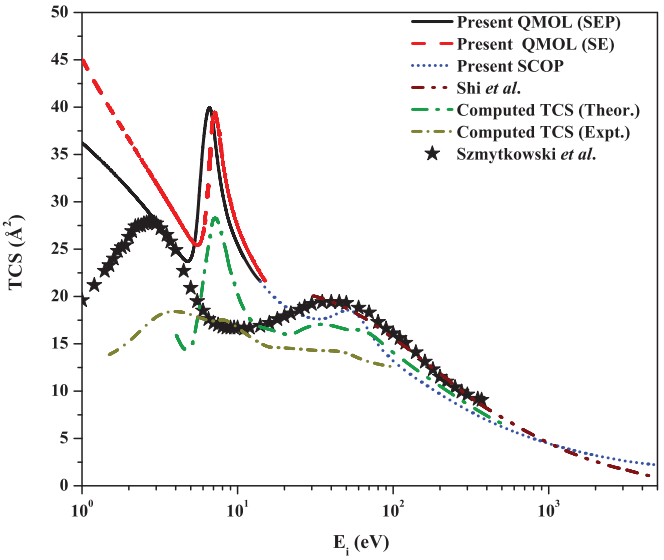

FIG. 4. (Color online) Total cross section for e-NF_3 scattering in Å^2. Solid line, present QMOL (SEP); dashed line, present QMOL (SE); dotted line, present SCOP; dash-dot dotted line, Shi *et al.* [7]; dash dotted line, computed TCS (Theor.) [6] (see text for details); short dash dotted line, computed TCS (Expt.) [6] (see text for details); stars, Szmytkowski *et al.* [6].

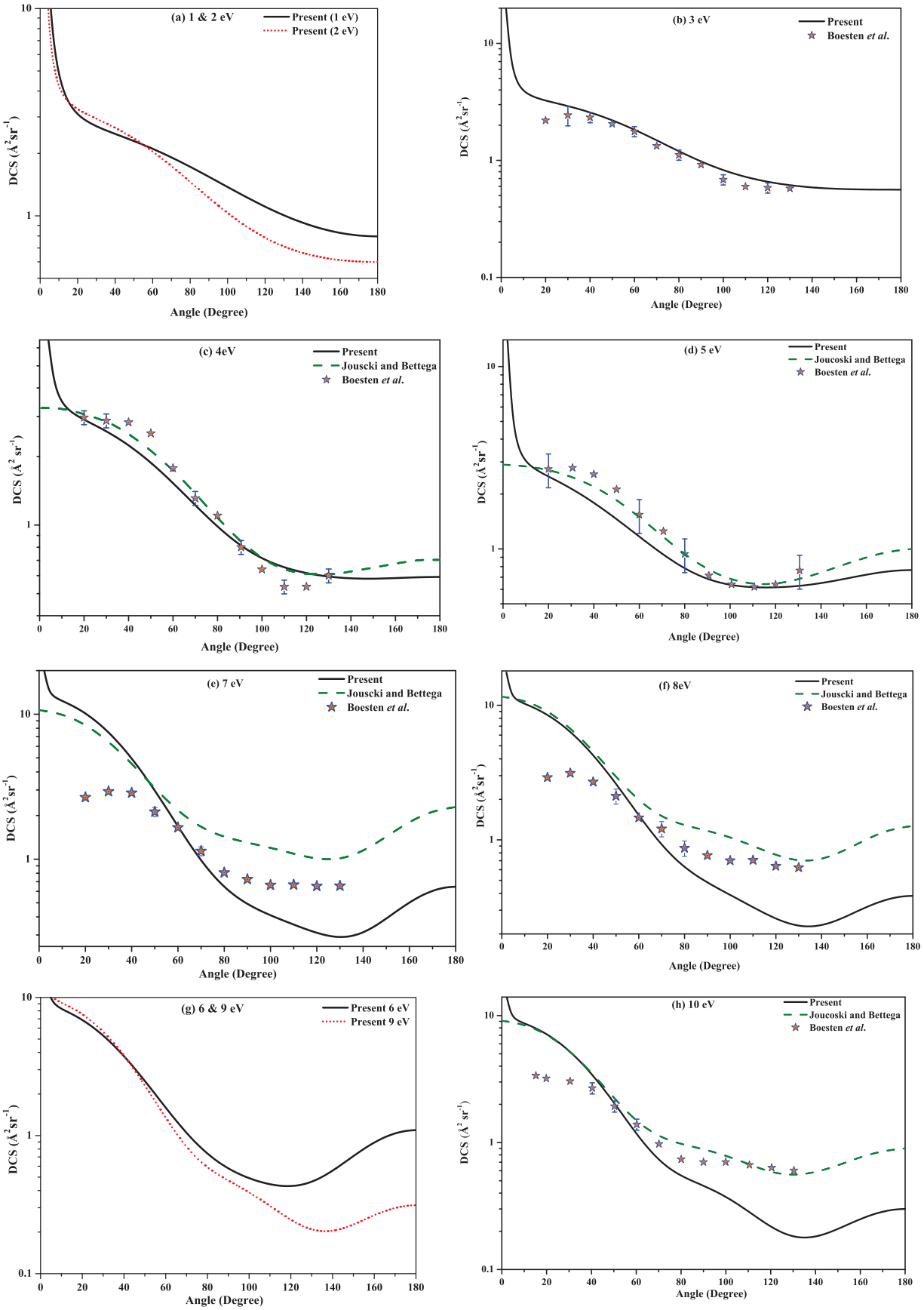

FIG. 5. (Color online) DCSs for e-NF_3 scattering at different energies. Solid or dotted line, present; dashed line, Joucoski and Bettega [11]; stars, Boesten *et al*. [10].

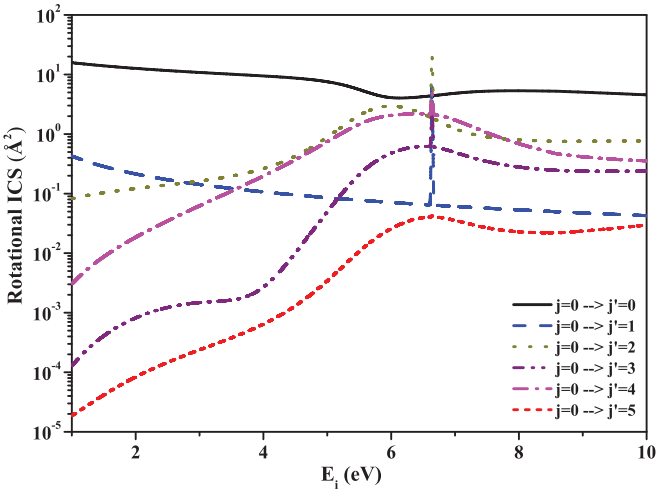

FIG. 6. (Color online) Rotational excitation cross sections for e-NF_3 scattering.

the computed TCS (Theor.). The overall shape of present data matches quite nicely with the computed TCS (Theor.). However, computed TCS (Theor.) underestimates present data. This may be attributed to the inclusion of ionization cross section instead of inelastic cross section in this TCS. The exceptionally lower value of computed TCS (Expt.) may be resulted from the relatively high uncertainty of ∼30% in the normalization procedure of Boesten *et al*. [10].

At energies above 10 eV, the present TCS shows reasonable agreement with the available data [6,7]. Present TCS shows a hump at the same energy region spanning from 20 to 100 eV as observed in the TCS curve of Szmytkowski *et al*. [6] and in the computed TCS (Theor.). After 100 eV the present TCS monotonically decreases and merges with the available experimental and theoretical data [6,7].

Qualitatively, the present result shows good agreement with the computed TCS (Theor.) throughout the energy range and with the measurement of Szmytkowski *et al*. [6].

Figure 5 shows the results of the differential cross section for NF_3 by electron impact from 1 to 10 eV. DCSs beyond 10 eV (up to 30 eV) are available from the authors, but not included here for brevity. The graphs are shown for 1–10 eV along with the available experimental and theoretical results. For 3, 4, and 5 eV the present data show excellent agreement with the experimental data of Boesten *et al*. [10]. However, as the incident energy increases above 5 eV, the present data show some discrepancies for a backward peak at an angular range from 80° to 130°, but matches well below 80° at the forward peak for 7, 8, and 10 eV. The theoretical cross section of Joucoski and Bettega [11] shows agreement with the experimental data of Boesten *et al*. [10] above 5 eV, below which it shows deviation from the experiment. This can be attributed to the polarization effect, which they have not included in their calculation. However, in the present case the polarization effect was incorporated in the calculation, which is strongest at short range, while at intermediate and long range polarization is weak. This might be the reason behind the apparent lower value of present DCSs at large angles. For 1, 2, 6, and 9 eV no previous data are available for comparison. More experimental investigation is required for NF_3 to quantify the results computed using different methods.

TABLE III. TCS for e^--NF_3 scattering.

Energy (eV)	TCS (Å²) (QMOL)	Energy (eV)	TCS (Å²) (SCOP)
1.0	36.23	14	21.59
1.5	33.48	15	20.97
2.0	31.32	20	18.91
2.2	30.56	30	17.43
2.4	29.84	40	17.72
2.6	29.16	50	18.82
2.8	28.51	60	18.16
3.0	37.70	70	16.30
3.2	27.28	80	14.87
3.4	26.70	90	13.89
3.6	26.13	100	13.18
3.8	25.58	120	12.12
4.0	25.05	140	11.35
4.5	23.96	160	10.70
5.0	23.99	180	10.15
5.5	28.12	200	9.67
6.0	36.01	300	7.96
6.2	38.16	400	6.92
6.4	39.47	500	6.23
6.6	39.94	600	5.71
6.8	39.36	700	5.30
7.0	37.97	800	4.96
7.5	33.86	900	4.69
8.0	30.90	1000	4.46
9.0	28.11	1500	3.67
10	25.76	2000	3.19
11	24.26	3000	2.64
12	23.14	4000	2.36
13	22.26	5000	2.19

Figure 6 represents the calculated values of rotational excitation cross section for NF_3 by electron impact. Rotational excitations for $j = 0 \rightarrow 1,2,3,4$ show prominent peak coincident at 6.6 eV, which is close to the resonance position as reflected in the eigenphase sum diagram. Elsewhere the rotational elastic ($j = 0 \rightarrow 0$) cross section is largest.

IV. CONCLUSION

A comprehensive study of electron impact scattering with NF_3 molecule is presented in this article. This investigation comprises eigenphase sum diagram, electronic, and rotational excitations and total and differential cross sections. The target properties obtained in the present close coupling calculation is in very good agreement with the available values. Hence, the wave functions generated by the DZP basis set are considered reliable. The total cross section is presented over the energy range 1 eV to 5 keV by employing two formalisms: R matrix for low-energy and SCOP for intermediate to high-energy calculations, both spliced at 14 eV. At this overlapping energy, cross sections from both theories match very well. In the low-energy region, shape resonances are detected at 5.6 and 6.2 eV by studying the eigenphase sum diagram. A broader enhancement is observed between 30 and 100 eV. The present

TCS shows qualitative as well as quantitative agreement with the sum of available theoretical elastic and ionization cross sections. Electronic and rotational excitations cross sections calculated by the *R*-matrix method are presented which are quite difficult to measure experimentally. The present DCSs show very good agreement with the available measurement of Boesten *et al*. [10] up to 5 eV, and after this energy the comparison is generally good for forward angles only.

There are no theoretical data available in the literature on the TCS for NF_3 over such a wide energy domain. The present work calls for more stringent theoretical investigation and further advancement in experimental attempt on this technologically relevant molecule to infer more information regarding its interaction with electron.

ACKNOWLEDGMENT

B.A. is pleased to acknowledge the support of this research by the Department of Science and Technology (DST), New Delhi through Grant No. SR/FTP/PS-27/2009.

[1] J. M. Veilleux, M. S. El-Genk, E. P. Chamberlin, C. Munson, and J. FitzPatrick, J. Nucl. Mater. **277**, 315 (2000).
[2] V. M. Donnelly, D. L. Flamm, W. C. Dautremont-Smith, and D. J. Werder, J. Appl. Phys. **55**, 242 (1984).
[3] M. J. Shaw and J. D. C. Jones, Appl. Phys. **14**, 393 (1977).
[4] J. I. Robson, L. K. Gohar, M. D. Hurley, K. P. Shine, and T. J. Wallington, Geophys. Res. Lett. **33**, L10817 (2006).
[5] P. Forster, V. Ramaswamy, P. Artaxo, T. Berntsen, R. Betts, D. W. Fahey, J. Haywood, J. Lean, D. C. Lowe, G. Myhre, J. Nganga, R. Prinn, G. Raga, M. Schulz, and R. Van Dorland, in *Climate Change 2007: The Physical Science Basis. Contribution of Working Group I to the Fourth Assessment Report of the Intergovernmental Panel on Climate Change,* edited by S. Solomon, D. Qin, M. Manning, Z. Chen, M. Marquis, K. B. Averyt, M. Tignor, and H. L. Miller (Cambridge University Press, Cambridge, 2006).
[6] C. Szmytkowski, A. Domaracka, P. Mozejko, E. Ptasinska-Denga, L. Klosowski, M. Piotrowicz, and G. Kasperski, Phys. Rev. A **70**, 032707 (2004).
[7] D. H. Shi, J. F. Sun, Z. L. Zhu, and Y. F. Liu, Eur. Phys. J. D **57**, 179 (2010).
[8] M. A. Rahman, S. Gangopadhyay, C. Limbachiya, K. N. Joshipura, and E. Krishnakumar, Int. J. Mass Spectrom. **319-320**, 48 (2012).
[9] T. N. Rescigno, Phys. Rev. A **52**, 329 (1995).
[10] L. Boesten, Y. Tachibana, Y. Nakano, T. Shinohara, H. Tanaka, and M. A. Dillon, J. Phys. B **29**, 5475 (1996).
[11] E. Joucoski and M. H. F. Bettega, J. Phys. B **35**, 783 (2002).
[12] P. D. Haaland, C. Q. Jiao, and A. Garscadden, Chem. Phys. Lett. **340**, 479 (2001).
[13] V. Tarnovsky, A. Levin, K. Becker, R. Masner, and M. Schmidt, Int. J. Mass Spectrom. Ion Proc. **133**, 175 (1994).
[14] H. Deutsch, T. D. Mark, V. Tarnovsky, K. Beckerc, C. Cornelissen, L. Cespiva, and V. Bonacic-Koutecky, Int. J. Mass Spectrom. Ion Proc. **137**, 77 (1994).
[15] J. Tennyson, Phys. Rep. **491**, 29 (2010).
[16] A. Barot, D. Gupta, M. Vinodkumar, and B. Antony, Phys. Rev. A **87**, 062701 (2013)
[17] B. Goswami, R. Naghma, and B. Antony, Mol. Phys. (2013) doi: 10.1080/00268976.2013.766369.
[18] R. Naghma, B. N. Mahato, M. Vinodkumar, and B. K. Antony, J. Phys. B **44**, 105204 (2011).
[19] CCCBDB at http://cccbdb.nist.gov.
[20] S. E. Novick, W. Chen, M. R. Munrow, and K. J. Grant, J. Mol. Spectrosc. **179**, 219 (1996).
[21] A. L. McClellan, *Tables of Experimental Dipole Moments* (Freeman, San Francisco, 1963).
[22] A. M. Arthurs and A. Dalgarno, Proc. Phys. Soc. Lond. A **256**, 540 (1960).
[23] A. Faure, J. D. Gorfinkiel, L. A. Morgan, and J. Tennyson, Comput. Phys. Commun. **144**, 224 (2002).
[24] M. Gailitis, J. Phys. B **9**, 843 (1976).
[25] N. Sanna and F. A. Gianturco, Comput. Phys. Commun. **114**, 142 (1998).
[26] H. L. Cox and R. A. Bonham, J. Chem. Phys. **47**, 2599 (1967).
[27] S. Hara, J. Phys. Soc. Jpn. **22**, 710 (1967).
[28] X. Zhang, J. Sun, and Y. Liu, J. Phys. B **25**, 1893 (1992).
[29] D. Staszewska, D. W. Schwenke, D. Thirumalai, and D. G. Truhlar, Phys. Rev. A **29**, 3078 (1984).
[30] C. J. Joachain, *Quantum Collision Theory* (North-Holland, Amsterdam, 1983).
[31] N. Ruckhaberle, L. Lehmann, S. Matejcik, and E. Illenberger, J. Phys. Chem. A **101**, 9942 (1997).
[32] D. Nandi, S. A. Rangwala, S. V. K. Kumar, and E. Krishnakumar, Int. J. Mass Spectrom. Ion Proc. **205**, 111 (2001).